doi:10.1016/j.jmb.2007.04.056 J. Mol. Biol. (2007) 370, 331–348

JMB

Available online at www.sciencedirect.com

ScienceDirect

ELSEVIER

Molecular and Structural Basis for Redox Regulation of β-Actin

Ingrid Lassing[1]†, Florian Schmitzberger[2]†, Mikael Björnstedt[3] Arne Holmgren[2], Pär Nordlund[2], Clarence E. Schutt[4] and Uno Lindberg[1]*

[1]*Department of Microbiology Tumor Biology, and Cell Biology, Karolinska Institutet SE-171 77 Stockholm, Sweden*

[2]*Department of Medical Biochemistry and Biophysics Karolinska Institutet, SE-171 77 Stockholm, Sweden*

[3]*Division of Pathology F46 Department of Laboratory Medicine, Karolinska University Hospital, Huddinge, SE-141 86 Stockholm, Sweden*

[4]*Department of Chemistry Princeton University Princeton, NJ 08544-1009, USA*

**Corresponding author*

An essential consequence of growth factor-mediated signal transduction is the generation of intracellular H_2O_2. It operates as a second messenger in the control of actin microfilament dynamics, causing rapid and dramatic changes in the morphology and motile activity of stimulated cells. Little is understood about the molecular mechanisms causing these changes in the actin system. Here, it is shown that H_2O_2 acts directly upon several levels of this system, and some of the mechanistic effects are detailed. We describe the impact of oxidation on the polymerizability of non-muscle β/γ-actin and compare with that of muscle α-actin. Oxidation of β/γ-actin can cause a complete loss of polymerizability, crucially, reversible by the thioredoxin system. Further, oxidation of the actin impedes its interaction with profilin and causes depolymerization of filamentous actin. The effects of oxidation are critically dependent on the nucleotide state and the concentration of Ca^{2+}. We have determined the crystal structure of oxidized β-actin to a resolution of 2.6 Å. The arrangement in the crystal implies an antiparallel homodimer connected by an intermolecular disulfide bond involving cysteine 374. Our data indicate that this dimer forms under non-polymerizing and oxidizing conditions. We identify oxidation of cysteine 272 in the crystallized actin dimer, likely to a cysteine sulfinic acid. In β/γ-actin, this is the cysteine residue most reactive towards H_2O_2 in solution, and we suggest plausible structural determinants for its reactivity. No other oxidative modification was obvious in the structure, highlighting the specificity of the oxidation by H_2O_2. Possible consequences of the observed effects in a cellular context and their potential relevance are discussed.

Keywords: ADP-β-actin; antiparallel dimer; cysteine sulfinic acid; H_2O_2; thioredoxin

Introduction

In many eukaryotic cells redox effects appear to have central roles in signal transduction, and H_2O_2 is essential for growth factor-induced signaling, since reactive oxygen species (ROS) quenching abolishes it.[1] Intracellular H_2O_2 is transiently generated upon activation of receptors for peptide growth factors and cytokines as well as integrin-mediated cell adhesion. It acts as a rapidly produced and effective second messenger, whose spatiotemporal presence in cells often correlates with changes in the microfilament system.[2,3]

Growth factor-stimulated H_2O_2 production is also closely interrelated with increases in the intracellular concentration of Ca^{2+},[4] and appears to correspond to the kinetics of actin polymerization-dependent outgrowth of lamellipodia and filopodia.[5,6]

Actins are highly conserved eukaryotic proteins existing in different cellular isoforms. Non-muscle

† I.L. and F.S. contributed equally to this work.

Abbreviations used: DTNB, 5,5′-dithiobis(2-nitrobenzoic acid); DTT, 1,4-dithiothreitol; Gdn-HCl, guanidine hydrocloride; ROS, reactive oxygen species; Trx, thioredoxin; TR, thioredoxin reductase.

E-mail address of the corresponding author: uno.lindberg@ki.se

β-actin and γ-actin, amongst the most abundant proteins in many cell types, are pivotal in maintaining and mediating the infrastructure of the cellular matrix. They form an essential part of chemo-mechanical transduction systems in non-muscle cells, where they, together with actin-binding proteins, generate force for various activities involved in translocation and cell shape change.

The constant and rapid reorganization of the actin microfilament system during cell motility and migration, mitogenesis, and phagocytosis depends on nucleation, elongation, and depolymerization of actin filaments as elementary processes.[6,7] The dynamic reorganization of cellular actin is highly regulated, and ROS appear to be one vital regulatory element.[2] Experiments have indicated that actin could constitute a direct target for oxidative modification *in vivo*.[8–10] Moreover, actin was shown to be oxidatively modified in pathophysiological states suggestive of oxidation as a cause of mechanical dysfunction.[11,12] Thus, an explanation of the molecular basis of redox-regulated microfilament processes requires an understanding of the mechanism of assembly/disassembly and related changes of actin during redox conditions as well as its regulation by associated proteins.

Most of the research on actin has been dedicated to characterizing its attributes under reducing conditions. Equally important is an understanding of its properties in an oxidizing environment, representative of the circumstances during signal transduction by H_2O_2. Experiments to study an effect of oxidation on actin *in vitro* have been done with muscle α-actin,[13] whereas the non-muscle β/γ-actins would seem to be the more relevant isoform with respect to cell shape and motility. Indeed, one of the few significant differences between α-actin and β/γ-actin is the number of cysteine residues, the thiol groups of which are the protein moieties generally most reactive towards H_2O_2. Non-muscle β and γ-actins have six cysteine residues (Figure 1), and α-actin has five.

Here, we have examined the biochemical effects of oxidation by H_2O_2 on the capacity of the actin isoforms to form filaments and characterized the structural consequences of oxidation in β-actin.

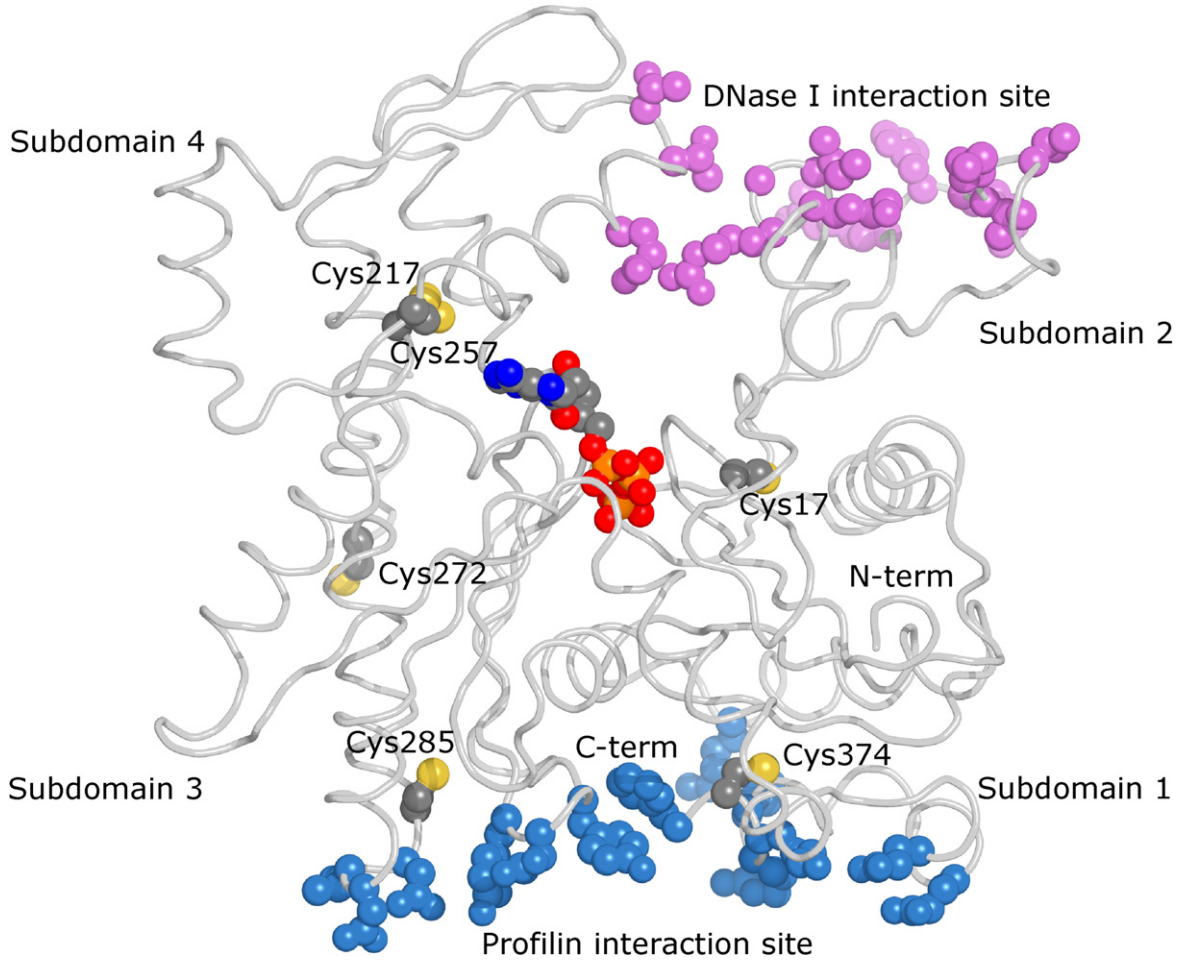

Figure 1. Illustration of the position of cysteine residues and the profilin and DNase I interaction sites in actin. The C^{α} atom cartoon represents the β-actin structure.[17] The color scheme for this and the following model illustrations, unless stated otherwise, is as follows. Ball-and-stick representation for the atoms: carbon, grey; nitrogen, blue; oxygen, red; phosphorus, orange; sulfur, yellow. Amino acid residues involved in the interaction with DNase I (derived from the α-actin–DNase I complex[104]) are colored magenta and those in contact with profilin are colored light-blue.

The results show that oxidation by H_2O_2 has profound and differential effects on both monomeric and filamentous non-muscle actin, and can lead to the formation of disulfide-linked antiparallel homodimers.

Results

Actin thiol groups and their reactivity towards 5,5′-dithiobis(2-nitrobenzoic acid) (DTNB) and H_2O_2

The number of accessible SH-groups in α-actin and β/γ-actin in the presence of ATP or ADP (see Materials and Methods), is given in Tables 1 and 2. At high concentrations (0.1 mM) of Ca^{2+}, monomeric α-actin and β/γ-actin in the presence of both ATP and ADP had one and two accessible cysteine residues, respectively. At submicromolar concentrations of Ca^{2+}, an additional DTNB-reactive SH-group appeared in α-actin-ADP, as shown earlier.[14] Similarly, the ADP-form of β/γ-actins exposed an extra DTNB-reactive cysteine residue at 1 μM Ca^{2+}.

In the ATP-form of β/γ-actin, the additional SH-group was only partially accessible and, in the presence of 0.1 mM Ca^{2+}, its appearance required a higher concentration of H_2O_2 or prolonged incubation time. Thus, one of the three cysteine residues could not be oxidized by H_2O_2, even though it was accessible to DTNB. Notably, for the extra cysteine to become unavailable, it was sufficient to increase the concentration of Ca^{2+} to 10 μM, under otherwise similar conditions (Table 2).

Effect of oxidation on actin polymerizability

Oxidation of ATP-β/γ-actin with 5 mM H_2O_2 at 1 μM of Ca^{2+} (one cysteine oxidized) did not affect the lag phase or the steady-state level of polymerization significantly (Figure 2(a)). In contrast, oxidation of ADP-β/γ-actin at 1 μM Ca^{2+} (two cysteine residues oxidized) led to a complete loss of polymerizability (Figure 2(b)). Incubation of ADP-β/γ-actin with H_2O_2 with 0.1 mM Ca^{2+} (one cysteine oxidized; Table 2) resulted in an actin which polymerized more slowly but reached a steady-state level comparable to that of the non-oxidized control (data not shown). Similarly, oxidation of α-actin in the ADP form at 0.1 mM Ca^{2+}, for a prolonged period, led to decreased polymerizability (data not shown).

Table 1. Number of DTNB reactive SH-groups/actin molecule before and after oxidation with H_2O_2

	Total SH	SH groups in non-denatured actin
A. *In 0.1 mM Ca^{2+}*		
ATP-α-actin	5.0 ($n=1$)	1.0 ($n=1$)
ADP-α-actin	5.0 ($n=7$)	1.0 ($n=7$)
Oxidized		
ATP- α-actin	4.0 ($n=1$)	0.5 ($n=1$)
ADP-α-actin	4.1 ($n=4$)	0.5 ($n=3$)
ATP-β/γ-actin	5.9 ($n=3$)	2.0 ($n=3$)
ADP-β/γ-actin	6.0 ($n=8$)	2.0 ($n=4$)
Oxidized		
ATP-β/γ-actin	4.3 ($n=2$)	0.9 ($n=2$)
ADP-β/γ-actin	4.0 ($n=7$)	1.0 ($n=3$)
B. *In 1 μM Ca^{2+} (non ox.)*		
ADP-β/γ-actin	6.0 ($n=1$)	3.0 ($n=1$)
ATP-β/γ-actin	6.0 ($n=1$)	2.3 ($n=1$)

The total number of SH groups reactive towards DTNB was assayed in the presence of GdnHCl, and SH groups available in non-denatured monomers were analyzed in G-buffer. Oxidized samples were exposed to 20 mM H_2O_2 for 40 min at 37 °C.

Table 2. Effect of calcium on oxidation of cysteine residues in ADP-β/γ-actin

Oxidation conditions	$[Ca^{2+}]_{free}$ (μM)	Oxidized cysteine residues	
		Number	Identity
5 mM H_2O_2, 10 min, 25 °C	1	2	Cys272/Cys374
5 mM H_2O_2, 15 min, at 25 °C	10	0.6	Cys272
5 mM H_2O_2, 15 min, 37 °C	10	2.3	Cys272/Cys374
5 mM H_2O_2, 15 min, 37 °C	100	1	Cys272
20 mM H_2O_2, 40 min, 37 °C	100	2	Cys272/Cys374

Number of oxidized SH-groups after incubation with H_2O_2 in the presence of different concentrations of Ca^{2+}.

Effect of the thioredoxin system on oxidized ADP-β/γ-actin

The reversibility of oxidation by H_2O_2 and its effect on the polymerizability of ADP-β/γ-actin at 1 μM Ca^{2+} are illustrated in Figure 2. Oxidized protein was incubated with the thioredoxin system, which reduces disulfide bonds and cysteine sulfenic acids, products of oxidation of cysteine residues with H_2O_2. Indeed, thioredoxin rapidly reduced the oxidized cysteine residues in ADP-β/γ-actin. All components of the thioredoxin (Trx) system (NADPH, thioredoxin reductase (TR), and Trx; see Materials and Methods) were required for the reduction of the cysteine residues and subsequent restoration of the capacity of the protein to form polymers (Figure 2(d)). Incubation of ADP-β/γ-actin under more oxidative conditions (higher concentrations of H_2O_2, longer incubation time) led to a product that could not be reduced by the Trx-system, likely due to formation of cysteine sulfinic or sulfonic acids.

Molecular status of oxidized ADP-β/γ-actin

The molecular mass distribution of the non-polymerizable ADP-β/γ-actin, formed at 0.1 mM Ca^{2+} incubated with 20 mM H_2O_2 for 40 min, is illustrated in Figure 3(a). The protein was essentially recovered as a major peak at the position expected for monomeric actin, with smaller amounts of protein appearing next to it in the higher molecular mass region. The predominant monomeric nature of

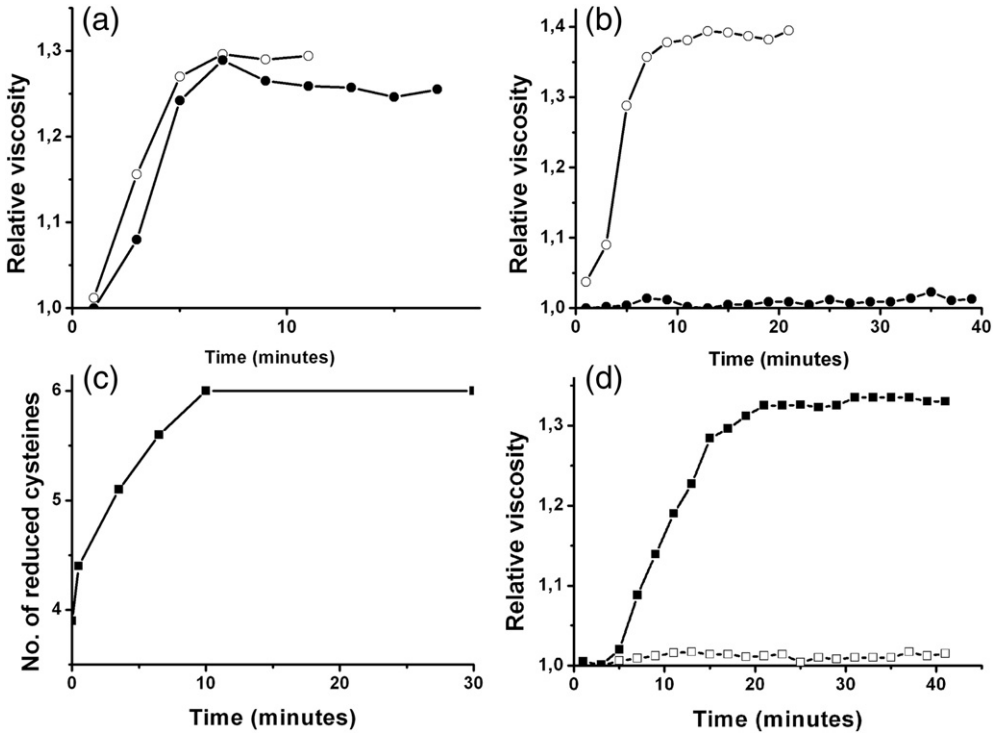

Figure 2. Effect of oxidation on actin polymerizability. (a) Polymerization of ATP-β/γ-actin (0.4 mg/ml) before (○) and after oxidation (●) with 5 mM H_2O_2 (see Materials and Methods). (b) Polymerization of ADP-β/γ-actin before and after oxidation with H_2O_2. Actin was incubated for 10 min with 5 mM H_2O_2 (oxidant not removed); symbols have the same meaning as in (a). (c) Reduction of oxidized cysteine residues with the Trx system. Upon removal of H_2O_2, oxidized ADP-β/γ-actin in G buffer with ADP and 50 μM Ca^{2+}, was incubated with the Trx system for increasing lengths of time and the number of SH groups was determined with DTNB in guanidine-HCl (see Materials and Methods). (d) Restoration of polymerizability of ADP-β/γ-actin inactivated by H_2O_2. Oxidized actin was incubated with the Trx system for 60 min at 37 °C, after which polymerization was induced by adding polymerizing salts at time zero and the viscosity was measured at 25 °C.

the oxidized ADP-β/γ-actin was confirmed by SDS-PAGE in the absence of reducing agents (see Figure 3(a) and (b)). The major peak had ~4 cysteine residues available for reaction with DTNB (i.e. two cysteine residues oxidized). In contrast, the actin in the higher molecular mass fraction contained ~2.0 cysteine residues available for DTNB in guanidine hydrochloride (Gdn-HCl), suggesting that a total of ~4 cysteine residues had been oxidized.

Similarly, gel-filtration of the oxidized, non-polymerizable ADP-β/γ-actin in the presence of polymerizing salts resulted in one major peak with monomeric actin, and a second peak of higher molecular mass. Approximately 90% of the applied protein was recovered, and the major peak contained more than ~60% of the applied protein, demonstrating that the monomeric form of oxidized actin remained in the non-polymerizable form. The actin sample from the major peak had two oxidized cysteine residues, in agreement with the results obtained under non-polymerizing conditions. Actin from this fraction could be concentrated to more than 15 mg/ml in G-buffer (see Materials and Methods) without the solution becoming viscous, confirming that the self-associating capacity of the actin monomers had been eliminated by oxidation.

ATP-induced polymerization of oxidized ADP-β/γ-actin

Intriguingly, addition of 0.5 mM ATP to oxidized ADP-β/γ-actin led to recovery of polymerizability, although polymer formation occurred after a considerable lag phase (Figure 4). Exposure of ADP-β/γ-actin to more oxidative conditions (higher concentrations of H_2O_2, longer times) resulted in a product that could not be recovered in a polymerizable form by the Trx system, again presumably indicating that cysteine sulfinic or sulfonic acids had formed. However, even after such treatment, ATP restored the polymerizability of the protein.

Interaction of oxidized ADP β/γ-actin with profilin and DNase I

In order to obtain information about potential changes in the structure of actin upon oxidation, its interactions with profilin and DNase I were studied. The results shown in Figure 5 illustrate the difference in affinity of non-oxidized and oxidized ADP-β/γ-actin for profilin. Here, the ADP-β/γ-actin samples were incubated with a twofold molar excess of profilin and then applied to poly-l-proline Sepharose resin, which binds profilin as well as

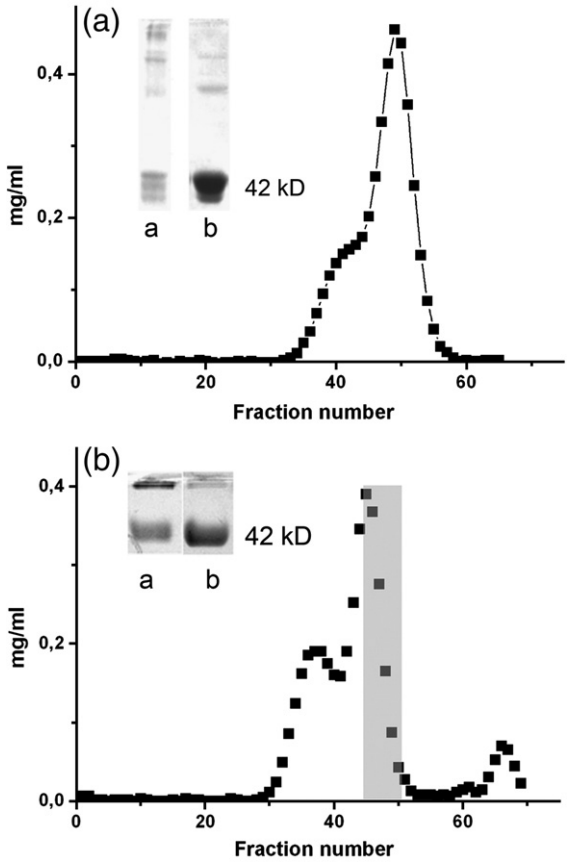

Figure 3. Size distribution of oxidized ADP-β/γ-actin. (a) Analysis of oxidized ADP- β/γ-actin by chromatography on S-300 in 5 mM KH_2PO_4/K_2HPO_4 (pH 7.6), 0.5 mM ADP, 0.1 mM $CaCl_2$, 10 μM EDTA. Inset: protein from fractions 39 (lane a) and 49 (lane b) after non-reducing SDS-PAGE (10% polyacrylamide gel) and stained with Coomassie brilliant blue (trace amounts of actin dimers, trimers etc. are seen above the oxidized actin monomers; no protein band was seen below the major actin band). (b) Chromatography of oxidized β-actin under polymerizing conditions. The shaded area indicates fractions used for crystallization. Inset: lane a fr. 39, lane b from shaded area.

profilin:actin complexes, but not actin alone. The major fraction of the non-oxidized actin bound to the poly-l-proline Sepharose, indicating stable complex formation, whereas oxidized actin was recovered mostly in the flow-through. These results demonstrate clearly that oxidation of ADP-β/γ-actin weakens its interaction with profilin. Notably, ADP-β/γ-actin with only one cysteine oxidized was retained by poly-l-proline Sepharose; i.e. its interaction with profilin was not affected significantly (data not shown).

The effect of oxidation of ADP-β/γ-actin on the binding to DNase I was analyzed with the DNase I inhibition assay.[15] Oxidation of two cysteine residues in ADP-β/γ-actin caused a two- to threefold increase in the K_d for the interaction with DNase I, suggesting that oxidation at the C terminus of the actin affected the interdomain relationship and conformation of the DNAse I interaction site of the actin molecule. However, oxidation of the most reactive cysteine did not influence the binding of DNase I.

Effect of H_2O_2 on filamentous actin

The effect of H_2O_2 on actin, polymerized to steady-state, was followed by monitoring the viscosity. The oxidant caused an immediate drop in viscosity of the solution (Figure 6(a)). Centrifugation of H_2O_2-treated samples at 30 psi (1 psi ≈6.9 kPa) for 30 min showed that almost all of the actin was in the supernatant (Figure 6(a)), suggesting that exposure to H_2O_2 had resulted in fragmentation or depolymerization of the filaments.

When pyrenyl-containing filaments were exposed to 5 mM H_2O_2, no significant change in the fluorescence could be detected, demonstrating that the filaments were not disassembled into monomers, but rather had become fragmented (see Figure 6(b)). Increasing the concentration of H_2O_2 to 20 mM, however, decreased the fluorescence to background levels within 2 h (Figure 6(c)), indicative of complete depolymerization.

Oxidation of filaments in the presence of a low concentration of Ca^{2+} (1 μM) did not seem to cause significant depolymerization, regardless of whether they had been formed in a low concentration of Ca^{2+}, or in 0.1 mM Ca^{2+}, with subsequent addition of EGTA to lower the concentration of Ca^{2+} (Figure 6(c)). However, at concentrations of Ca^{2+} above 10 μM, significant depolymerization did occur (data not shown).

Effect of diamide on SH groups and polymerizability of β/γ-actin

Incubation of eukaryotic cells with diamide, a relatively thiol-specific oxidizing agent, causes reorganization of the microfilament system.[16] Here, β/γ-actin incubated with equimolar amounts of diamide, which eliminated the DTNB-reactivity of one SH-group, still polymerized (Figure 7). However, incubation of the actin with a higher concentration of diamide, oxidizing two to four cysteine residues, significantly decreased the polymer-forming capability of the actin, in agreement with the results obtained with H_2O_2. In these cases, addition of ATP to the inactivated actin rapidly restored its polymerizability, except in the case where five out of six SH-groups had become oxidized.

Crystal structure of β-actin after incubation with H_2O_2

An ADP-β-actin sample, which had been incubated with 20 mM H_2O_2 and had retained its polymerization potential, was crystallized in the presence of ADP. The structure solution (Table 3) is consistent with four molecules, here referred to as A, B, C, and D, respectively, in the asymmetric unit. Interpretable electron density is present for the full-

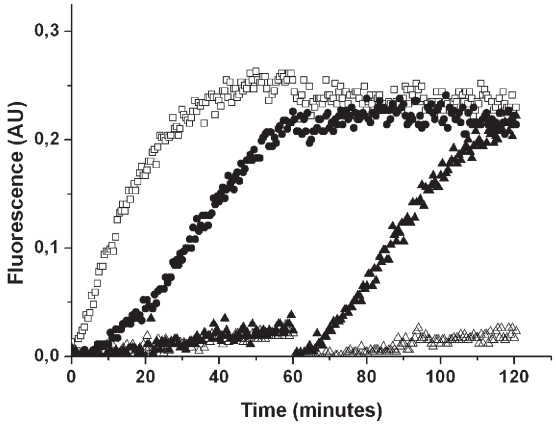

Figure 4. ATP-induced polymerization of oxidized ADP-β/γ-actin. The first part of the graph (0–60 min) represents the polymerization of non-oxidized actin in ADP (□), oxidized actin in ADP (△ and ▲), and oxidized ADP-actin, to which ATP was added before polymerizing salts (●). The second part shows that addition of 0.5 mM ATP restores the polymerizability of oxidized ADP-β/γ-actin, even after incubation for 60 min (▲). Addition of 0.5 mM DTT to oxidized ADP-actin after 60 min of incubation is shown (△). Polymerization of actin (0.4 mg/ml) was monitored by the pyrenyl-assay (see Materials and Methods).

length protein, except for residues 1–5 (1–3 in molecules B and C), 40–49 (DNase I binding loop), 372–375 in molecules A and C, as well as residue 375 in molecule B. At the nucleotide-binding site, contiguous electron density for the presumed position of three phosphate groups was visible after simulated annealing refinement in the initial σ^A-weighted omit map of the $2F_o–F_c$ type at a level of greater than the 3.0σ providing a convincing argument for the presence of an ATP, rather than an ADP, molecule. The presence of ATP in the actin molecule was unexpected. However, although β-actin was purified in the presence of ADP, a subfraction of β-actin with bound trace amounts of ATP could have been copurified and this sample crystallized. Alternatively, actin may have crystallized with ADP, in a closed state, and ADP then exchanged to ATP because of the greater affinity of actin for ATP. However, interpretable electron density for the histidine 73 methyl group, present in the profilin:β-actin structure was not observed.[17]

Superposition on previously solved actin structures demonstrates that, overall, the structure closely resembles those, except for the relative position of subdomain 2 in the open profilin:β-actin structure.[18] The actin is consequently in a conformation typically referred to as the closed state, and the four molecules in the asymmetric unit are conformationally congruent. However, this is the first time that this particular arrangement of the actin molecules has been observed. In the asymmetric unit, three protomers are oriented almost identically, whereas another molecule is located in an antiparallel orientation to them. Protomers B and D are related by a nearly 2-fold, non-crystallographic axis located between their C termini (angle of rotation 178°) and the interface between them buries a calculated solvent-accessible surface area of ~780 Å^2 per protomer (Figure 8(a)). Protomers A and C are arranged in an essentially identical way with a crystallographic 2-fold axis relating them to their counterpart molecules.

The interaction interface is composed of residues from subdomains 1 and 3,[19] and displays a mixed electrostatic character with ~60% non-polar atoms. In protomers B and D, the interface comprises residues 166–173 located in a loop in subdomain 3, which together with residues 286 and 289 (subdomain 3) line up against residues 350–355 located in an α-helix in subdomain 1 from the adjacent molecule. Apparent hydrophilic interactions include a hydrogen bond formed across the gap of the two molecules between the hydroxyl group of Tyr143 (subdomain 1) and the carboxyl group of Glu167 (subdomain 3). The interface further consists of residues 370–374 (subdomain 1), which are situated alongside the equivalent, mainly α-helical, range of the adjacent molecule.

Structural effects of oxidation by H_2O_2

Inspection of difference Fourier electron density maps indicated a covalent modification of cysteine 272 (Figure 9(a)) in all four molecules, essentially consistent with an oxidation to cysteine sulfenic or sulfinic acid. Modeling of either form agrees with the data and the corresponding real space density fit and cross-validated *R*-factor display no significant differences. Also, a cysteine sulfonic acid residue fits the electron density of the $2F_o–F_c$ type and no negative peaks in electron density maps of the $F_o–F_c$ type at below the −2.0σ contour level at the site of the modeled oxygen atoms became apparent. However, modeling of a sulfinic acid residue was

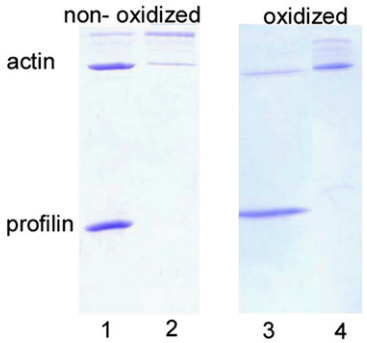

Figure 5. Interaction between profilin and actin, before and after oxidation of actin. Non-oxidized, and oxidized, actin was mixed with a twofold excess of profilin and then fractionated on a poly-l-proline Sepharose column. Fractions from the flow-through (lanes 2 and 4) show actin not interacting with profilin, and lanes 1 and 3 show the protein recovered from the matrix (profilin and profilin:actin) stained with Coomassie brilliant blue after SDS-PAGE (15% polyacrylamide gel).

eventually preferred, because of indications for such a form in positive difference Fourier peaks (Figure 9(a)). Nonetheless, it is not unlikely that the observed electron density represents a superposition of several oxidation states in the crystal, consistent with mass spectrometry analysis of the protein sample (data not shown). No significant conformational change in the protein is observable in the vicinity of cysteine 272, apart from the side-chain of glutamate 276. It is displaced from its corresponding position in the structure of profilin:β-actin,[17] which seems attributable to electrostatic repulsion with the oxygen atoms of the oxidized Cys272 in our β-actin structure (Figure 9(a)).

Upon reprocessing of the diffraction data using images, where radiation damage was less severe, contiguous electron density between the presumed position of the sulfur of Cys374 in molecules B and D could be interpreted as a disulfide bond (Figure 9(b)). It displays an architecture consistent with that of a right-handed conformation with most of the parameters refining close to the expected values.[20] However, the dihedral angle around the S–S bond refined to 132°, deviating from the energetically favorable 100°,[21] and the torsion angle around the Cα–Cβ bond in protomer B to 155°, deviating from the mean value of −60°. This may indicate an energetically less favorable conformation of the

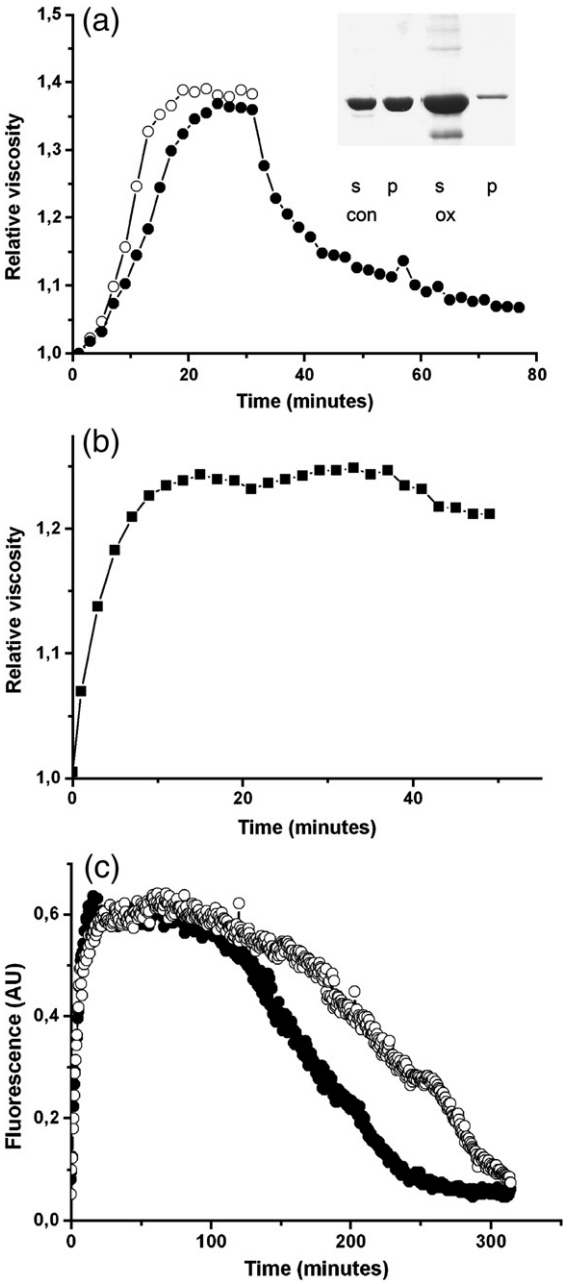

Figure 6. Effect of H_2O_2 on filamentous actin. (a) Polymerization of ADP-β/γ-actin (0.4 mg/ml) in G-ADP buffer (see Materials and Methods) at 0.1 mM Ca^{2+}, induced by the addition of polymerizing salts at time zero. After 32 min, 5 mM H_2O_2 (final conc.) was added and polymer formation was monitored by viscometry at 25 °C. Inset: Status of the actin after the drop in viscosity: 0.25 ml samples of the oxidized actin were centrifuged for 30 min in an airfuge at 30 psi at room temperature. Pelleted material and precipitated protein from the supernatant was resuspended in 0.2 ml of G-ADP buffer boiled with sample buffer, and analyzed by SDS-PAGE (10% polyacrylamide gel). The supernatant and pellet obtained with non-oxidized F-actin were used as a control. (b) Effect of adding 0.1 mM EGTA before polymerizing salt (final Ca^{2+}_{free} is 1 μM), and 5 mM H_2O_2 (final conc.) at 20 min, followed by the addition of 0.1 mM $CaCl_2$ at 40 min. (c) The effect of H_2O_2 on ADP-β/γ-actin polymers monitored by the pyrenyl assay (see Materials and Methods). For this, ADP-β/γ-actin (0.1 mM Ca^{2+}) was polymerized. In one sample, the Ca^{2+} concentration was lowered to 1 μM by the addition of 0.1 mM EGTA 45 min after initiation of polymerization (○). After 55 min, 5 mM H_2O_2 (final conc.) was added to both samples, and after 100 min 20 mM H_2O_2 (final conc.) was added.

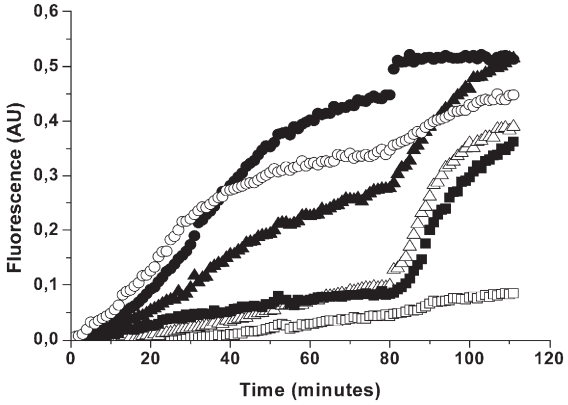

Figure 7. Effect of diamide on the polymerization of ADP-β/γ-actin. Diamide was added to the protein (0.5 mg/ml, 2% (w/v) pyrenyl-actin) in G-ADP buffer at 10 μM $CaCl_2$ to give final concentrations of diamide of 10 μM (●), 30 μM (▲), 0.1 mM (Δ), 1 mM (■), 10 mM (□), and the control without diamide (○) (total volume 200 μl). Polymerization was induced by addition of 2 mM $MgCl_2$ and 100 mM KCl. After 80 min, 2 μl of 0.5 M ATP was added to all samples and the reaction was followed for another 30 min. In a parallel experiment, the number of oxidized cysteine residues was determined by the DTNB method.

Table 3. Crystallographic data statistics

A. *Data collection and integration*	
Wavelength (Å)	1.0000
Space group	$C222_1$
Unit cell dimensions	
a (Å)	119.17
b (Å)	222.59
c (Å)	133.71
Resolution range (Å)	35-2.60 (2.68-2.60)
No. unique reflections (multiplicity)	52 031 (3.6)
R_{meas} [a]	0.15 (0.79)
Mean $\langle I \rangle / \sigma \langle I \rangle$	9.34 (1.72)
Completeness (%)	94.7 (76.4)
Wilson *B*-factor (Å^2)	39
B. *Refinement*	
R_{cryst} [b]	0.210 (0.279)
R_{free} [c]	0.288 (0.371)
No. reflections: working/test set	48 371/2548
Average refined *B*-factor (Å^2) [d]	42
No. non-H atoms	
Protein	11 028
Water	494
Ligand	161
C. *Model analysis*	
Estimated coordinate error (Å) [e]	0.37
r.m.s. deviation	
Bond lengths (Å) [f]	0.010
Bond angles (deg.) [f]	1.389
Ramachandran plot [g]	
No. residues in most favored region	1375
No. residues in generously allowed region	40
No. residues in disallowed region	0

Values in parentheses are for the highest resolution shell.

[a] $R_{meas} = \dfrac{\sum_h \sqrt{\frac{n_h}{n_h - 1}} \sum_i^{n_h} |\langle I_h \rangle - I_{h,i}|}{\sum_h \sum_i^{nh} I_{h,i}}$;

with $\langle I_h \rangle = \dfrac{1}{n_h} \sum_i^{n_h} I_{h,i}$ and n_h multiplicity.

[b] $R_{cryst} = \dfrac{\sum_h ||F_{obs}| - |F_{calc}||}{\sum_h |F_{obs}|}$; where F_{obs} and F_{calc} are the observed and calculated structure-factors respectively.

[c] R_{free}: cross-validation of R_{cryst}.[95]

[d] Total refined *B*-factor including the TLS component.

[e] Estimated coordinate error of the structure based on R_{free} as calculated by Refmac.[94]

[f] Calculated with Refmac.

[g] Calculated with MolProbity.[99]

disulfide bond and/or the onset of radiation damage.[22] The latter is supported by calculations of electron density maps using the data ranging from 90° to 180° (see Materials and Methods), where no interpretable contiguous electron density for the position of the disulfide bond was observable, likely symptomatic of the radiation sensitivity of it, its breakage, and subsequent mobility of the C termini.

The C-terminal five residues of molecules B and D are viewed down the rotational axis, oriented towards the protein part of the D protomer (Figure 8(a)). A similar arrangement may exist in molecules A and C. Although the electron density for residues C-terminal of His371 was not interpretable, plausibly an intermolecular disulfide bond with their counterpart molecule, related by the crystallographic 2-fold axis could be present.

Noticeably, the hydroxyl groups of four tyrosine residues, Tyr133 and Tyr169 from both molecules, are positioned around the disulfide bond (Figure 9(b)). The oxygen atoms of the hydroxyl groups of Tyr169 are at a distance of ~4 Å and ~4.5 Å, respectively, from the closest sulfur atom (with the valency state of sulfur in the disulfide bond corresponding to a van der Waals radius of ~1.8 Å), whereas those of Tyr133 are at a distance of ~5 Å and ~6.5 Å, respectively. In the crystal structure of oxidized β-actin these are the only hydrophilic protein moieties, apart from backbone carbonyl groups and amides, in the immediate vicinity of the disulfide bond.

No other oxidative modification was obvious, suggesting that the applied concentration of H_2O_2 was not excessive. It is notable that Cys217 and Cys257, which are in close proximity in the structure, did not seem to be affected. Likely, this is a reflection of the specificity of the oxidation.

Discussion

Cys272–the most reactive cysteine

Oxidative modifications of cysteines in response to transmembrane signaling has emerged as a highly relevant regulatory and reversible mechanism of central function in a wide variety of systems.[23,24] Here, we show that exposure of non-muscle ADP-β/γ-actin to H_2O_2 at high concentrations of Ca^{2+} (0.1 mM) in G-buffer results in the oxidation of one cysteine, and that a second cysteine is modified by prolonged incubation with H_2O_2 at higher temperature. Importantly, it is only after the second cysteine had been oxidized that an interference with the polymerizability of the protein and its binding to profilin was observed. Since chemical modification of Cys374 by various means affects polymerizability and profilin binding by the actin,[25] these results imply that another cysteine in non-muscle actin reacts more readily than Cys374, and that this is Cys272. Consistently, our crystal structure revealed that Cys272 is oxidized and displays a higher oxidation state than Cys374, showing it to be the most reactive cysteine in β-actin. Significantly, in α-actin and non-vertebrate actin isoforms the amino acid in position 272 is alanine and no cysteine is present in the structurally equivalent location.

Reactivity of Cys272: structural considerations

The intrinsic reactivity of thiol groups is modulated by their chemical microenvironment and by the extent to which they are accessible to reactive groups. In β-actin, the oxidized Cys272 is located at the surface of the protein, is solvent-exposed (Figure 9(a)), and therefore easily accessible to H_2O_2 in monomeric or dimeric actin. The only notable pro-

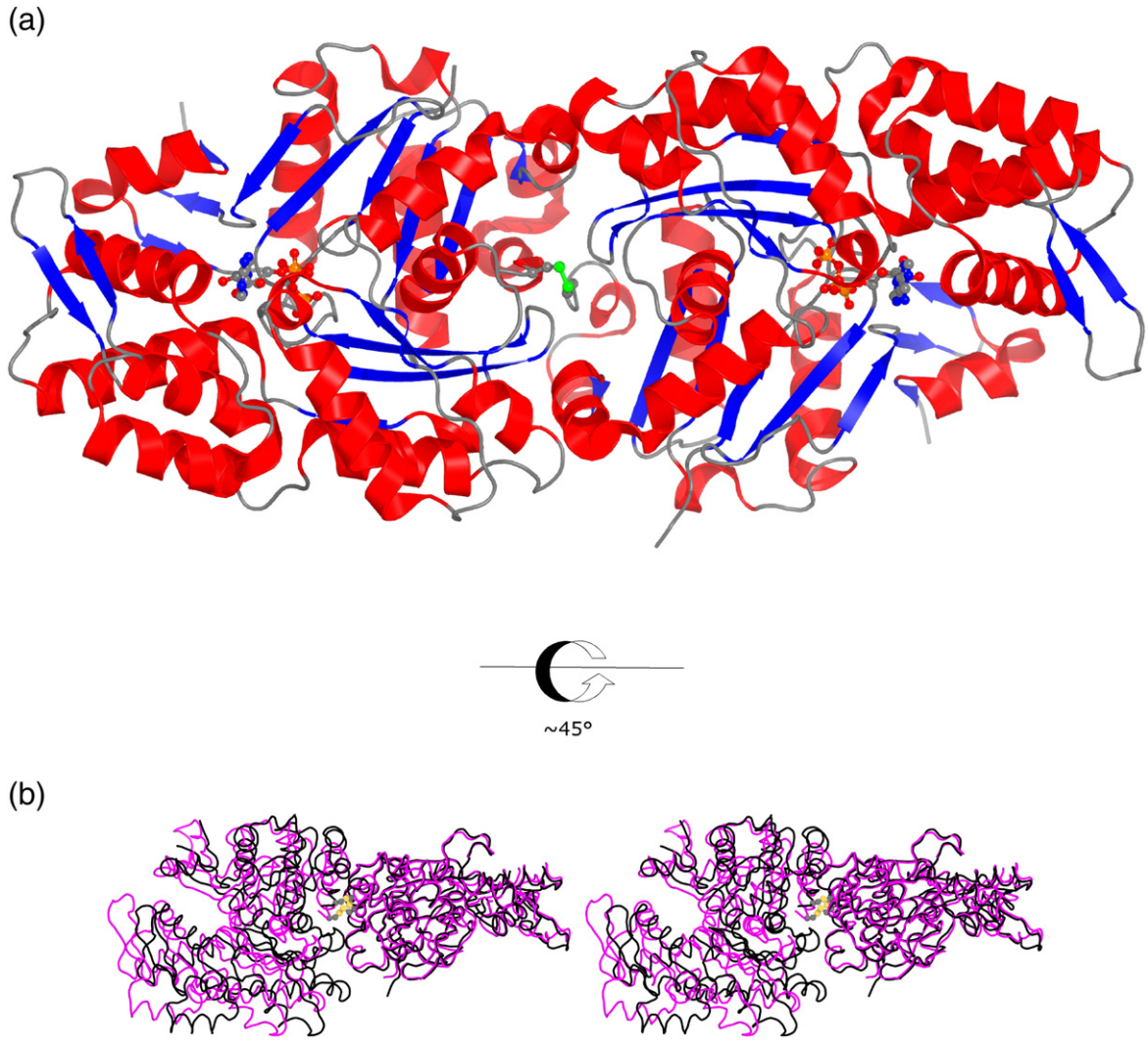

Figure 8. Illustration of the antiparallel β-actin homodimer. (a) Secondary structure representation of the β-actin dimer in an orientation with the approximately 2-fold non-crystallographic axis approximately perpendicular to the plane of the paper. The disulfide bond (green) and the ATP molecule are shown in ball-and stick-representation. Color scheme: red, α-helices; blue, β-strands; grey, loops. (b) Stereo-representation of the structural variability of the β-actin homodimer (black, without ligands) and the superimposed α-actin dimer[49] (magenta, without ligands) *via* the protomer to the right. The disulfide bond is shown in ball-and-stick representation for both dimers.

tein moieties in the microenvironment of Cys272 are the side-chains of Glu276 and Asn280. A cysteine thiol would be expected to have a pK_a near 9 and largely protonated at physiological pH, and thus have a low reactivity. While the microenvironment of Cys272 does not appear to lower the pK_a value of Cys272, the removal of the thiol proton in the reaction might be facilitated by the carboxyl group of Glu276. An activation mechanism involving an aspartate/glutamate and a catalytic cysteine has been proposed for proteins of the thioredoxin-like family, where the carboxyl moieties are thought to assist in deprotonation of the thiol group of the reactive cysteine.[26,27] In β-actin, Glu276 might play a role in the reaction with H_2O_2 in mediating proton transfer to generate a leaving water molecule. Moreover, in solution the effect of metal ions on the reactivity of Cys272, though not directly inferable from our data, cannot be excluded.

Oxidation of Cys374 and the exposure of Cys17

It is known from studies on α-actin that the highly conserved Cys374 is available for reaction with various types of thiol reagents, and that manipulation of the C terminus affects the ability of the protein to form polymers.[25,28,29] However, the mechanism by which the C terminus is involved in monomer–monomer interactions during filament assembly is not known. Yet, there is evidence for a reciprocal allosteric communication between the C terminus and both the nucleotide-binding site and the DNase I interaction site within the actin molecule.[25,30–32] In this respect, it is worth pointing out that the C terminus with the carboxyl group of Phe375, in the conformation observed in molecule D in our crystal structure, forms a hydrogen bonding interaction with the backbone nitrogen atom of Ile136. This residue, in turn, is situated next

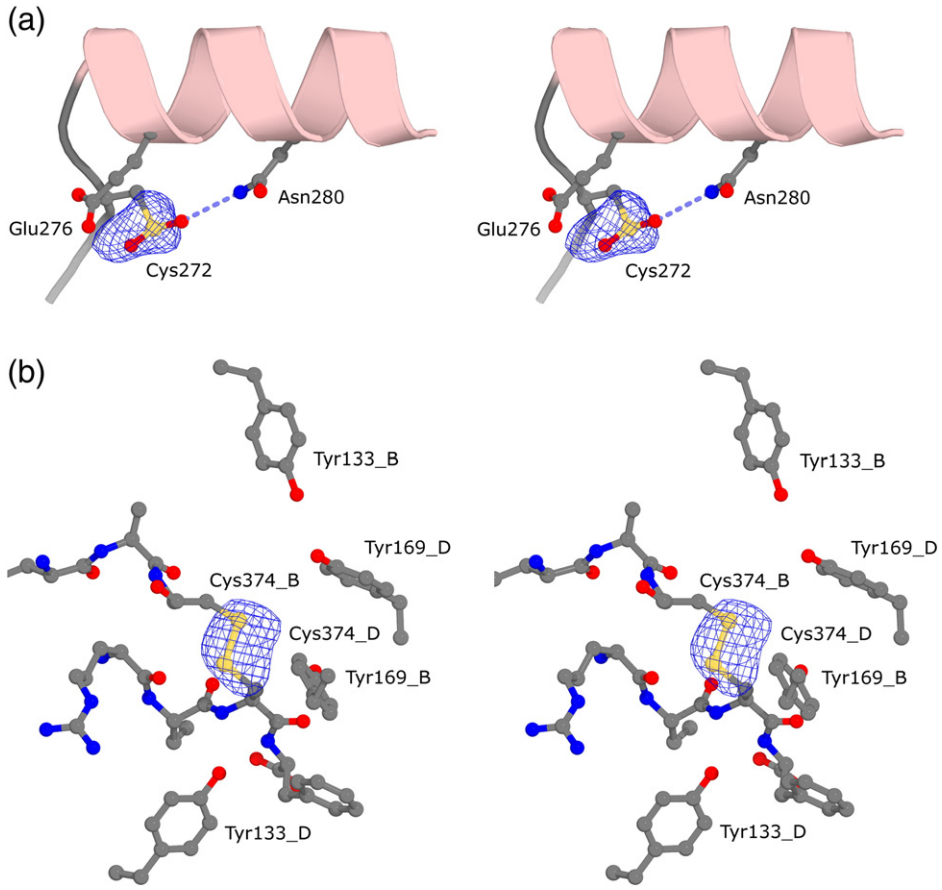

Figure 9. Illustration of the effects of oxidation on Cys272 and Cys374 in the β-actin structure. (a) Stereo-representation of the omit electron density with mF_o–DF_c coefficients contoured at 3.0σ (0.13 e^-/A^3, blue) before modeling the side-chain oxygen atoms of sulfinic acid and the final refined cysteine sulfinic acid model. A potential hydrogen bonding interaction of one of the sulfinic acid oxygen atoms of oxidized Cys272 with Asn280 is indicated by a broken light blue line. (b) Stereo-representation of the omit electron density with mF_o–DF_c coefficients contoured at 3.7σ (0.15 e^-/A^3, blue) before modeling the sulfur atoms and the final refined disulfide bond coordinates. Amino acid residues at the C termini and in the vicinity of the disulfide bond are shown.

to Gln137, proposed to form the hinge point for domain motions in the actin molecule,[19] and potentially involved in ATP hydrolysis. Of note, the carboxyl group of Phe375 in the oxidized structure, positioned this deep in the hydrophobic pocket, has not been observed in other actin crystal structures, where instead the corresponding space is occupied by water molecules or co-crystallized ligands. This interaction may constitute a contact point between the C terminus and the nucleotide-binding site, and in this way relay changes from the C terminus to the DNase I interaction site *via* the nucleotide-binding site, explaining how different chemical modifications of Cys374 alter the properties of actin.

Faulstich and co-workers showed that at low concentrations of Ca^{2+}, modification of Cys374 in ADP-α-actin results in a slow, reversible conformational transformation, exposing a second cysteine, identified as Cys10.[14] Additionally, the presence of ATP or metal ions in concentrations sufficient for binding to moderate-affinity sites shielded Cys10.

Here, it is shown that non-muscle ADP-β/γ-actin also has a DTNB-reactive cysteine, in addition to Cys272 and Cys374, accessible at low levels (1 μM) of Ca^{2+} but shielded at increased concentrations of Ca^{2+} (>10 μM) and not oxidized by H_2O_2. Amino acid residue 10 in non-muscle actins is valine. However, Cys17 occupies a similar position in the interior of subdomain 1. The appearance of an additional DTNB-reactive cysteine at low concentrations of Ca^{2+} in the absence of ATP suggests strongly that Cys17 is exposed *via* a conformational change similar to that occuring in α-actin under these conditions. The high degree of flexibility in this region of the molecule is of particular interest, since alterations in the structure are expected to affect the configuration and/or position of the DNase I binding loop crucial for the formation of actin filaments. The fact that chemical modification of Cys374 influences Cys17 provides further evidence for a communication between the C terminus and the DNase I binding loop.[25,30–32] Significantly, our present results imply that these conformational changes are under Ca^{2+} control.

Oxidation of Cys374: Ca^{2+} sensitivity and loss of polymerizability

The reversibility of the inactivation of the polymer-forming capacity of ADP-β/γ-actin caused by H_2O_2 at low concentrations of Ca^{2+} implies that the structural changes associated with this effect may be physiologically relevant. Notably, Ca^{2+} at concentrations above 10 μM shields Cys374 from the oxidative effects of H_2O_2, including exposure of Cys17. Stimulation of cells with various kinds of agonists, such as growth factors and cytokines, is almost invariably linked to increases in the intracellular concentration of Ca^{2+}, from submicromolar values in resting cells to more than 10 μM.[33] It is within this concentration range that calcium ions modify the sensitivity of actin to H_2O_2.

Interestingly, mere addition of ATP, even to the over-oxidized form, restored the capacity of actin to polymerize, showing that ATP is effective at restoring interdomain connectivity and the normal positioning of subdomain 2 involved in filament formation.

Cys272, Cys374 and the actin filament

Clearly, Cys374 of actin is of importance from a regulatory point of view. Changes in its availability upon polymer formation and effects of chemical modification of this residue on polymerizability and stability of the actin polymer[25,28,29] indicate a high degree of flexibility of the C terminus of the protein, and that the penultimate Cys374 has an important role in establishment of intermonomer contacts. During polymerization, Cys374 on one monomer is near residue 41 in subdomain 2 and residues 262–274,[31,34,35] comprising the "hydrophobic plug", allegedly involved in stabilizing the interstrand relationship in the actin filament.[36] Thus, intermonomer interactions would be expected to be destabilized by oxidation of Cys374, a reaction that, as shown here for β-actin, results in depolymerization.

H_2O_2 influences the organization of actin microfilaments and motility of many eukaryotic cells, which are known to contain significant amounts of glutathionylated actin. It is conceivable that oxidation of both Cys272 and Cys374 with subsequent glutathionylation could be important in the disassembly of filaments as the environment becomes more oxidative during a shift in the reduced/oxidized glutathione (GSH/GSSH) equilibrium. Furthermore, oxidative modification of Cys272 might alter the interaction of filamentous actin with actin-binding proteins.

Disulfide bond: architecture and environment

In the crystal structure of the oxidized β-actin, Cys374 in protomers B and D are engaged in an intermolecular disulfide bond, which is partly solvent-accessible in the crystal lattice. The disulfide bond appears to be in an energetically unfavorable state and susceptible to breakage by radiation-induced radicals.[22,37]

The protein context of the disulfide bond in the oxidized β-actin structure is largely hydrophobic, with the exception of the hydroxyl groups of Tyr133 and Tyr169. It has been pointed out that hydroxyl groups or aromatic rings through interactions with the disulfide bond confer stability and restrict accessibility to reducing agents.[20,38]

Cys374 is partially solvent-accessible in monomeric and filamentous actin.[36,39] It is oriented towards the protein interior in most monomeric actin structures having intact C termini.[17,40–42] In this orientation, the aromatic ring of Tyr133 may be involved in π-bonding to the sulfur of Cys374, which are at a distance of 3.4–4.0 Å in these structures. Sulfur–π aromatic interactions have been suggested to modulate the reactivity of cysteine residues.[43] Alternatively, Arg116 is a potential residue involved in facilitating the reactivity of Cys374, as it is situated in its proximity in many actin structures.

Antiparallel homodimer formation

The interaction between actin molecules B and D in the crystal is consistent with an antiparallel β-actin homodimer connected *via* an intermolecular disulfide bond (Figures 8 and 9). In solution, α-actin antiparallel dimers, inferred to be cross-linked *via* Cys374, have been observed.[44–48] However, from comparison of the crystal structures (Figure 8(b)) it would appear that the discrepancies in interatomic distances between the reported dimers could be due to the inherent structural plasticity rather than fundamentally different species.

Oxidized β-actin in our preparations is predominantly in the monomeric form in solution. Even so, the presence of an antiparallel dimer in the crystal implies that a subpopulation existed in the preparations of oxidized actin (see Figure 3; higher molecular mass species). Consequently, the dimer is arranging under non-polymerizing conditions. Previously, it was shown that an antiparallel dimer can assemble during different polymerizing conditions.[45,49] However, the driving force for its origination seems to be the tendency of actin to form a disulfide bond *via* Cys374 due to oxidation of its sulfur atom. This is consistent with reports that slow thiol oxidation of monomeric α-actin by atmospheric oxygen gives rise to disulfide-bonded antiparallel dimers.[48] In the presence of crosslinking reagents, oxidized Cys374 may react readily with those, which then may restrict certain functional conformational changes.[44] In light of our observations, it seems conceivable that the observed disulfide bond in the α-actin antiparallel dimer did form due to oxidation of a fraction of non-cross-linked α-actin, present together with cross-linked protein.[49] The modeled intermolecular disulfide bond in α-actin homodimer crystal structures appeared to be susceptible to breakage by synchroton radiation or refined to an unfavorable torsion

angle, corroborating our argument for the general lability of the intermolecular disulfide bond in actin dimers of this kind.[49–51]

Implications of an antiparallel dimer formed under oxidizing conditions

Transient interactions are increasingly being recognized as crucial in modulating protein–protein recognition and function in regulatory and signal transduction processes.[52] The cellular significance of an antiparallel dimer is unclear. The apparent lability of the dimer assembly and the disulfide bond implies that the association represents a non-permanent interaction. Thus, the antiparallel dimer may play a role as a rapidly activated regulatory component, reactive and reversible towards changes in the oxidative environment. A dimer interaction could be generally unstable but, upon formation of a disulfide bond, become more lasting under oxidizing conditions, such as signal transduction by H_2O_2.

The *in vitro* formation of disulfide-bonded antiparallel actin dimers might be important for understanding cellular redox responses to growth factor or integrin stimulation, including branching of filaments within lamellipodia of motile cells.[7] The advancement of a cell edge depends on polymerization of actin, formation of dynamic filament ensembles, and disassembly of the actin filaments. During the process of lamellipodia formation, the multiprotein complex Arp2/3 appears to be engaged in nucleation of branches, though the exact mechanism by which Arp2/3 causes filaments to branch is unknown.[53] In electron microscopy images, long, unbranched filaments are the dominating structures in lamellipodia, and bundles of long seemingly unbranched filaments constitute the core of filopodia, suggesting that more than one mechanism exists for the formation of actin filaments in advancing cell edges.

Integration of an entire antiparallel β-actin dimer, in the conformation observed in the crystal, into a single helical actin filament is not compatible with the polarity of the filament. However, it has been demonstrated that antiparallel α-actin dimers become integrated into growing actin filaments *in vitro* and participate directly in actin filament growth.[48,54] Small protrusions at intervals along the filaments were observed by electron microscopy, suggesting that one of the protomers of the dimer had been incorporated into the filaments. Evidence for branched filaments was also detected, reminiscent of the branching filaments seen in the leading edge of highly motile cells. One could imagine that incorporated dimer sites constitute platforms for the binding of Arp2/3 to commence the formation of daughter filaments. It is possible that the inherent flexibility around the disulfide bond of a filament-integrated antiparallel dimer would necessitate actin-binding proteins to stabilize a defined structural state. Thus, Arp2/3 could enforce a particular conformation of the dimer to facilitate directed growth of the filament at a particular angle. Since the actin filaments further away from an advancing cell edge are long and apparently unbranched,[6] there must be a mechanism for remodeling the filaments within a short time-span.[7,55] If, as suggested here, the Arp2/3 were bound to the junction formed by an antiparallel dimer, dissociation of the branched filaments could be achieved by reduction of the disulfide bond in a more reducing environment, further away from the cell edge. Such a mechanism could explain the fact that *in vitro*, branches form primarily on newly formed filaments, rather than on older ones.[7] In the absence of actin-binding proteins, mechanical strain on the unstable disulfide bond, produced by the branched filaments, may suffice to break it, consistent with the observation of debranching of filaments with integrated antiparallel dimers.[54]

H_2O_2 and the impact on the actin microfilament system

ROS appear to be required effectors in the control of actin-based activities in various cell types.[2,3] However, a central question is whether ROS act directly on actin *in vivo*. Recent redox proteomics studies detected actins amongst the most prominent proteins oxidized in response to exposure of cells to oxidants.[8–10] Given our observations about the profound mechanistic impact of H_2O_2 on actin *in vitro*, we reason that *in vivo* a direct redox control of actin could be one of the most important processes regulating the dynamics of the microfilament system. Indeed, observation of a direct interaction *in vivo* between ROS and actin was reported recently.[8]

Clearly, for H_2O_2 to play a role in signaling to the microfilament system, its site of production must be localized near the system, because efficient reduction systems, such as glutathione peroxidase, peroxiredoxins, and catalase rapidly eliminate H_2O_2.[56] An initial oxidative burst would first have to overcome such oxidative defenses and necessitate amplification.[57] However, a H_2O_2 gradient may also have differential oxidative effects of functional relevance, leading to dimer formation, glutathionylation, and depolymerization in the actin system, depending on the location of the actin molecules, the source of the oxidant, the availability of surrounding reducing systems, and the presence of glutathione.

The major sources of ROS within both phagocytotic and non-phagocytotic cells are NAD(P)H oxidase-like protein complexes and lipoxygenase. Both function downstream of cytokine receptors,[58,59] and a direct interaction of their components with actin was confirmed.[60,61] These enzyme complexes are membrane-associated and activated by association with the GTPase Rac,[62] over-expression of which leads to increased levels of ROS in endothelial cells.[63] Consistently, ROS generation was inhibited by over-expression of a dominant negative form of Rac1.[64] In turn, in all cell types examined so far, Rac serves as a pivotal regulator of actin assembly and seems to determine where and when actin polymerizes.[65] Association with guanine nucleotide exchange

factors appears to target Rac1 to the membrane where, in migrating cells, actin reorganization also appears to be maximal, and causes its concomitant, spatially restricted activation.[66] Amplification of an H_2O_2 signal *in vivo* seems to occur through the integration of the Rac and phosphatidylinositol lipid kinase pathways.[57] Increased phosphorylation, through oxidative inhibition of phosphatases, is a hallmark of H_2O_2 signaling, and H_2O_2 is known to downregulate PTEN by oxidation, leading to increased formation of lipid kinase products (phosphatidylinositol 4,5 bisphosphate, PIP2 and the 3,4,5-trisphosphate, PIP3).[67] These phosphoinositides, in turn, appear to target guanine nucleotide exchange factors to the membrane, thus activating Rac1.[68]

Consequently, the impact of Rac on the actin-containing network *in vivo*, in addition to its apparent protein interaction-mediated role,[69] could be rationalized to a significant extent by its induction of the generation of ROS. This may explain Rac activities previously assumed to be unrelated, such as activation of lipoxygenase and NAD(P)H oxidase-like protein complexes and actin reorganization. The potential role of ROS as initiators and central molecules in the process may not have been appreciated sufficiently, since research into the signaling cascades has focused primarily on identifying protein–protein interactions, mostly under reducing conditions.

The formation of PIP2 caused by binding of agonists to cell-surface receptors in platelets peaks in 5–10 s after the addition of agonists.[70,71] Hydrolysis of PIP_2 releases inositol trisphosphate, which in turn releases Ca^{2+} from cytosolic stores with about the same kinetics.[71] Lamellipodia 2–4 μm long grow out in about 30–60 s after addition of agonists as seen with platelets and serum-starved cells.[72,73] Accumulation of PIP_2 in the plasma membrane in local areas, lipid rafts, could bind profilin:actin, with the consequent release of actin monomers in the neighborhood of the PIP_2-producing centers.[74,75] At the same time, the receptor-associated mechanisms could deliver increasing amounts of H_2O_2 into the advancing cell edges, although maximal concentration of the oxidant is not reached until 5–10 min after addition of a growth factor, and later in spreading cells.[1,76] The peak of H_2O_2 is reached long after initial waves of PIP_2-formation, Ca^{2+} release,[33] and polymerization of actin have passed, and at a time when depolymerization has become a significant contributor to steady-state turnover of filaments in advancing cell edges.

It is plausible that in the early phase of oxidation, the release of monomeric actin from profilin:actin, interacting with PIP_2 in the periphery of the cell, becomes involved in actin dimer formation, and that Arp2/3-dependent polymerization of actin involves dimer incorporation into filaments, augmenting branch formation. It is not inconceivable that in the later phase, when the H_2O_2 level is at a maximum, glutathionylation and depolymerization of filaments potentiate the turnover of filaments. Relatively little is known about the mechanism of actin filament disassembly *in vivo*. The *in vitro* results shown here suggest that the possibility of oxidation of filaments as a step in the depolymerization should be given serious consideration.

In conclusion, the evidence suggests strongly that many aspects of the actin response to various cellular stimuli occur under oxidizing conditions. This view is further strengthened by observations that a perturbed oxidative balance with increased ROS levels seems to be symptomatic of a number of disease types as well as cellular senescence.[77,78] Over-oxidation may have severe consequences, as oxidative damage is surmised to occur in neurodegenerative diseases.[79] Actin oxidation was elevated in brain extracts of patients with Alzheimer's disease,[80] actin glutathionylation was increased in cells of patients with Friedreich's ataxia,[11] and disulfide-linked actin oligomers in post-ischemic reperfusion in rat hearts were reported.[12] In autism, a serious neurobiological condition, neuronal migration defects and synaptic deficiencies have been suggested as the causes of hippocampal and amygdalar dysfunctions. PTEN, discussed above in connection with it being the link between oxidation by H_2O_2 and Rac, is implicated in the etiology of autism and would appear to exert its influence on brain development *via* the actin microfilament system.[81]

The relevance of ROS action on the actin system *in vivo* remains to be determined. Our results provide a basis for an understanding of the effect of H_2O_2 on the microfilament. Undoubtedly, future studies will have to take into account also the effect of ROS on actin in conjunction with actin-binding proteins.

Materials and Methods

Chemicals

ATP and ADP were from Roche; Hypatite C was from Clarkson Chromatography Products, South Williamsport, PA; DTT was from Saveen Werner AB; guanidine-HCl was from Fluka; and *N*-(1-pyrene) iodoacetamide was from Molecular Probes. All other chemicals were from Sigma. The purity of ADP was confirmed by chromatography on Mono Q resin (GE Healthcare). Thioredoxin and thioredoxin reductase were produced in *Escherichia coli*.[82] Vivaspin protein concentrators were from Vivascience.

Preparation of actin and profilin

Calf thymus profilin:actin was prepared and profilin and actin were isolated as described.[83] Filamentous actin was disassembled by extensive dialysis against 5 mM Tris-HCl (pH 7.6), 0.2 mM ATP, 0.1 mM $CaCl_2$, 10 μM EDTA, 0.5 mM DTT at 4 °C, and finally gel-filtered using Sephacryl S-300 (S-300, HR, GE Healthcare, Sweden) equilibrated with G-buffer (5 mM KH_2PO_4/K_2HPO_4 (pH 7.6), 0.5 mM ATP, 0.1 mM $CaCl_2$, 10 μM EDTA). To lower the concentration of free Ca^{2+} to micromolar levels, 0.1 mM EGTA was added to the buffer. For preparation of ADP-actin the S-300 column was equilibrated with G-buffer containing 0.5 mM ADP. Before experiments, DTT was removed by filtration on PD-10 columns (GE Healthcare, Sweden) or by S-300

chromatography equilibrated with G-buffer without DTT. In some experiments, actin was kept in G-buffer containing 50 μM $CaCl_2$. α-Actin from rabbit muscle was prepared as described,[84] and subjected to S-300 chromatography as above. Concentrations of actin were determined spectrophotometrically.[85] SDS-PAGE was performed with or without reducing agents.[86]

Determination of SH groups

Protein thiol groups were determined using DTNB and applying a molar extinction coefficient of 13,600 $M^{-1}cm^{-1}$ at 412 nm (A_{412}).[87] The total number of reduced thiol groups was verified by mixing one volume of actin (7–20 μM) with five volumes of DTNB in guanidine hydrochloride (Gdn-HCl). DTNB was dissolved in 99.5% (v/v) ethanol (10 mM) and mixed in a 1:9 (v/v) ratio with 6 M Gdn-HCl in 0.2 M Tris (pH 8.0). The background signal was established by mixing one volume of G-buffer with five volumes of DTNB in Gdn-HCl. Accessible thiol groups in the folded protein in G-buffer were determined by mixing one volume of actin sample (7–20 μM) with six volumes of 0.5 mg/ml DTNB in G-buffer, while monitoring A_{412} for 8 min.

Oxidation and reduction of actin

Oxidation of actin for preparative work was performed by incubating the protein with H_2O_2, after which the oxidant was removed by passing over a PD10 or an S-300 column equilibrated with G-buffer (4 °C). The polymerizability of oxidized ADP-actin and ATP-actin was analyzed by incubating 0.4–0.5 mg/ml protein in 10 mM KH_2PO_4/K_2HPO_4 (pH 7.6), 0.1 mM $CaCl_2$, 0.1 mM EGTA, 10 μM EDTA, supplemented with 0.2 mM ADP or ATP, respectively, with 5 mM H_2O_2 for 45 min at 25 °C. Then, polymerizing salts were added to a concentration of 2 mM $MgCl_2$ and 100 mM KCl, and the change in viscosity at 25 °C was monitored. Reduction was performed by incubating the actin with the Trx-system (2 μM thioredoxin, 50 nM thioredoxin reductase, 0.2 mM NADPH) at 37 °C for the lengths of time indicated. A sample containing the Trx-system components in G-buffer was used to determine their contribution of DTNB-reacting thiol groups.

Actin polymerization

Actin polymerization was monitored by high-shear viscometry at 25 °C using a Cannon-Manning viscometer, with a buffer flow-time of 60 s and a sample volume of 0.7 ml. Filament formation was also recorded using the pyrene assay with 2% pyrene-labeled β/γ-ADP-actin.[88] Pyrene-labeled actin was isolated by gel-filtration on an S-300 chromatography column equilibrated with G-buffer containing ADP. Polymerization was induced by addition of polymerizing salts as indicated in the Figure legends.

Crystallization of oxidized ADP-actin

Isolation of profilin:β-actin was performed as described above. Fractions eluted from the column were immediately supplemented with ATP and the protein was precipitated with 80% (w/v) $(NH_4)_2SO_4$ and stored at 4 °C. The ADP-form of β-actin was prepared as described above. The protein was then incubated with 20 mM H_2O_2 at 37 °C for 40 min and finally passed over an S-300 column in 5 mM Tris-HCl (pH 7.6), 0.5 mM ADP, 0.1 mM $CaCl_2$, 10 μM EGTA, 100 mM KCl. Actin from fractions 45–50 (Figure 3(b)) was concentrated to 5 mg/ml. Crystals were grown at 4 °C in hanging drops (Linbro plates), mixing equal volumes of protein (5 mg/ml) and crystallization buffer (0.1 M Hepes (pH 7.5), 1.6 M $(NH_4)_2SO_4$, 0.1 M NaCl). Crystals with maximal dimension of 140 μm appeared after about three months. They were transferred to a cryo-solution (0.1 M Hepes (pH 7.5), 1.8 M $(NH_4)_2SO_4$, 0.1 M NaCl, 0.1 M KCl, 1 mM $CaCl_2$, 10 mM ADP) with 5% (v/v) glycerol, and then to a cryo-solution containing 25% (v/v) glycerol, with incubation periods of 1–5 min for both.

Diffraction data processing, structure solution, and refinement

Crystals, mounted in cryoloops, were flash-frozen in liquid N_2. X-ray diffraction data, extending to ~2.45 Å resolution, were measured from a single crystal at −173 °C, in 180 frames of 1° increment, at the X06SA PXI beamline (Swiss Light Source) with a Mar225 CCD detector. Reflections were indexed and integrated with XDS and scaled in XSCALE.[89] A decrease in the intensity of the higher-resolution reflections and a marked deterioration of the data-merging statistics with increasing data collection time were indicative of significant radiation damage. Data conversion into structure factor amplitudes and subsequent format adaptions were performed with programs of the CCP4 suite (version 6.0.0-2).[90] The crystal structure was determined by molecular replacement using Phaser[91] with the protein part of α-actin (PDB-code 1J6Z) as a search model.[92] Data processing is consistent with space group $C222_1$ with four molecules in the asymmetric unit. Crystallographic rigid body refinement and torsion-angle molecular dynamics simulated annealing refinement with a slow-cooling protocol starting at 4726 °C (5000 K) with CNS,[93] using diffraction data to 2.5 Å resolution were followed by restrained, isotropic *B*-factor refinement with Refmac.[94] A 5% test set of randomly selected reflections was used for cross-validation throughout refinement,[95] which was iterated by manual rebuilding cycles in $\sigma^{\mathbf{A}}$-weighted electron density maps with COOT.[96] Correction of the amino acid sequence register for β-actin, addition of ligands, non-crystallographic symmetry averaging with differential weighting for variable parts, and refinement of protein domain-specific TLS parameters improved the data fit.[97] Refinement parameters for ATP, sulfate, and Ca^{2+} were retrieved from the CCP4 library,[90] and those for cysteine sulfinic acid, added in progressed refinement cycles, were generated with PRODRG.[98] Refinement was continued until convergence of the cross-validated *R*-factor. It was then realized that the electron density at the C termini of two molecules was potentially indicative of a disulfide bond. The data were reprocessed including only the first 90° of data (to 2.6 Å resolution), where radiation damage was less severe. Using the same reflection indices as before for cross-validation, simulated annealing refinement was performed (as described above), with the previously refined model and residues C-terminal of His371 removed (Table 3). Analogously, data from 90–180° were processed separately and the model refined with (data not shown).

Model analysis

The protein model was evaluated with MolProbity,[99] SFCHECK,[100] and WHATCHECK.[101] Structural superposition was done with LSQKAB.[90] Surfaces were

analyzed with the Protein-Protein interaction server,[102] PISA,[103] and programs of the CCP4 suite. Molecular representations were prepared with PyMol‡.

Protein Data Bank accession number

Atomic coordinates and structure factors for the protein model have been deposited in the RCSB Protein Data Bank with accession code 2OAN.

Acknowledgements

We are grateful to Ingegärd Andersson for technical assistance, and Terese Bergfors for introducing I.L. to protein crystallization. Herwig Schüler for help in determining the K_d for the interaction of oxidized actin and DNase I. We thank Andreas Kohl and Damian Niegowski for help with the diffraction data collection. This work was performed at the Swiss Light Source, Paul Scherrer Institut, Villigen, Switzerland. We are grateful to the machine and beamline groups, whose outstanding efforts have made these experiments possible. This work was supported by grants from the Swedish Cancer Society to I.L., F.S., A.H., P.N., and U.L, and by a grant from Magnus Bergvall foundation to I.L. Funding from the Swedish research council to P.N. and U.L., and from the Nancy Lurie Marks Family Foundation to C.E.S. is acknowledged.

References

1. Sundaresan, M., Yu, Z. X., Ferrans, V. J., Irani, K. & Finkel, T. (1995). Requirement for generation of H2O2 for platelet-derived growth factor signal transduction. *Science*, **270**, 296–299.
2. Moldovan, L., Mythreye, K., Goldschmidt-Clermont, P. J. & Satterwhite, L. L. (2006). Reactive oxygen species in vascular endothelial cell motility. Roles of NAD(P)H oxidase and Rac1. *Cardiovasc. Res.* **71**, 236–246.
3. Chiarugi, P. & Fiaschi, T. (2007). Redox signalling in anchorage-dependent cell growth. *Cell Signal*, **19**, 672–682.
4. Hong, J. H., Moon, S. J., Byun, H. M., Kim, M. S., Jo, H., Bae, Y. S. *et al.* (2006). Critical role of phospholipase Cgamma1 in the generation of H2O2-evoked [Ca2+]i oscillations in cultured rat cortical astrocytes. *J. Biol. Chem.* **281**, 13057–13067.
5. Watanabe, N. & Mitchison, T. J. (2002). Single-molecule speckle analysis of actin filament turnover in lamellipodia. *Science*, **295**, 1083–1086.
6. Small, J. V., Stradal, T., Vignal, E. & Rottner, K. (2002). The lamellipodium: where motility begins. *Trends Cell Biol.* **12**, 112–120.
7. Pollard, T. D. & Borisy, G. G. (2003). Cellular motility driven by assembly and disassembly of actin filaments. *Cell*, **112**, 453–465.
8. Fiaschi, T., Cozzi, G., Raugei, G., Formigli, L., Ramponi, G. & Chiarugi, P. (2006). Redox regulation of beta-actin during integrin-mediated cell adhesion. *J. Biol. Chem.* **281**, 22983–22991.
9. Fratelli, M., Demol, H., Puype, M., Casagrande, S., Eberini, I., Salmona, M. *et al.* (2002). Identification by redox proteomics of glutathionylated proteins in oxidatively stressed human T lymphocytes. *Proc. Natl Acad. Sci. USA*, **99**, 3505–3510.
10. Lind, C., Gerdes, R., Hamnell, Y., Schuppe-Koistinen, I., von Lowenhielm, H. B., Holmgren, A. & Cotgreave, I. A. (2002). Identification of S-glutathionylated cellular proteins during oxidative stress and constitutive metabolism by affinity purification and proteomic analysis. *Arch. Biochem. Biophys.* **406**, 229–240.
11. Pastore, A., Tozzi, G., Gaeta, L. M., Bertini, E., Serafini, V., Di Cesare, S. *et al.* (2003). Actin glutathionylation increases in fibroblasts of patients with Friedreich's ataxia: a potential role in the pathogenesis of the disease. *J. Biol. Chem.* **278**, 42588–42595.
12. Canton, M., Neverova, I., Menabo, R., Van Eyk, J. & Di Lisa, F. (2004). Evidence of myofibrillar protein oxidation induced by postischemic reperfusion in isolated rat hearts. *Am. J. Physiol. Heart Circ. Physiol.* **286**, H870–H877.
13. Dalle-Donne, I., Rossi, R., Milzani, A., Di Simplicio, P. & Colombo, R. (2001). The actin cytoskeleton response to oxidants: from small heat shock protein phosphorylation to changes in the redox state of actin itself. *Free Radic. Biol. Med.* **31**, 1624–3162.
14. Drewes, G. & Faulstich, H. (1991). A reversible conformational transition in muscle actin is caused by nucleotide exchange and uncovers cysteine in position 10. *J. Biol. Chem.* **266**, 5508–5513.
15. Blikstad, I., Markey, F., Carlsson, L., Persson, T. & Lindberg, U. (1978). Selective assay of monomeric and filamentous actin in cell extracts, using inhibition of deoxyribonuclease I. *Cell*, **15**, 935–943.
16. Blikstad, I. & Carlsson, L. (1982). On the dynamics of the microfilament system in HeLa cells. *J. Cell Biol.* **93**, 122–128.
17. Schutt, C. E., Myslik, J. C., Rozycki, M. D., Goonesekere, N. C. & Lindberg, U. (1993). The structure of crystalline profilin-beta-actin. *Nature*, **365**, 810–816.
18. Chik, J. K., Lindberg, U. & Schutt, C. E. (1996). The structure of an open state of beta-actin at 2.65 Å resolution. *J. Mol. Biol.* **263**, 607–623.
19. Page, R., Lindberg, U. & Schutt, C. E. (1998). Domain motions in actin. *J. Mol. Biol.* **280**, 463–474.
20. Petersen, M. T., Jonson, P. H. & Petersen, S. B. (1999). Amino acid neighbours and detailed conformational analysis of cysteines in proteins. *Protein Eng.* **12**, 535–548.
21. Perahia, D. & Pullman, B. (1971). The conformational energy map for the disulphide bridge in proteins. *Biochem. Biophys. Res. Commun.* **43**, 65–68.
22. Schmidt, B., Ho, L. & Hogg, P. J. (2006). Allosteric disulfide bonds. *Biochemistry*, **45**, 7429–7433.
23. Forman, H. J., Fukuto, J. M. & Torres, M. (2004). Redox signaling: thiol chemistry defines which reactive oxygen and nitrogen species can act as second messengers. *Am. J. Physiol. Cell Physiol.* **287**, C246–C256.
24. Kwon, J., Lee, S. R., Yang, K. S., Ahn, Y., Kim, Y. J., Stadtman, E. R. & Rhee, S. G. (2004). Reversible oxidation and inactivation of the tumor suppressor

‡ http://www.pymol.org

PTEN in cells stimulated with peptide growth factors. *Proc. Natl Acad. Sci. USA*, **101**, 16419–16424.
25. Aspenstrom, P., Schutt, C. E., Lindberg, U. & Karlsson, R. (1993). Mutations in beta-actin: influence on polymer formation and on interactions with myosin and profilin. *FEBS Letters*, **329**, 163–170.
26. Chivers, P. T. & Raines, R. T. (1997). General acid/base catalysis in the active site of Escherichia coli thioredoxin. *Biochemistry*, **36**, 15810–15816.
27. LeMaster, D. M., Springer, P. A. & Unkefer, C. J. (1997). The role of the buried aspartate of Escherichia coli thioredoxin in the activation of the mixed disulfide intermediate. *J. Biol. Chem.* **272**, 29998–30001.
28. Stournaras, C., Drewes, G., Blackholm, H., Merkler, I. & Faulstich, H. (1990). Glutathionyl(cysteine-374) actin forms filaments of low mechanical stability. *Biochim. Biophys. Acta*, **1037**, 86–91.
29. Pelikan Conchaudron, A., Didry, D., Le, K. H., Larquet, E., Boisset, N., Pantaloni, D. & Carlier, M. F. (2006). Analysis of tetramethylrhodamine-labeled actin polymerization and interaction with actin regulatory proteins. *J. Biol. Chem.* **281**, 24036–24047.
30. Mossakowska, M., Moraczewska, J., Khaitlina, S. & Strzelecka-Golaszewska, H. (1993). Proteolytic removal of three C-terminal residues of actin alters the monomer-monomer interactions. *Biochem. J.* **289**, 897–902.
31. Crosbie, R. H., Miller, C., Cheung, P., Goodnight, T., Muhlrad, A. & Reisler, E. (1994). Structural connectivity in actin: effect of C-terminal modifications on the properties of actin. *Biophys. J.* **67**, 1957–1964.
32. Kim, E., Wriggers, W., Phillips, M., Kokabi, K., Rubenstein, P. A. & Reisler, E. (2000). Cross-linking constraints on F-actin structure. *J. Mol. Biol.* **299**, 421–429.
33. Singh, D. K., Kumar, D., Siddiqui, Z., Basu, S. K., Kumar, V. & Rao, K. V. (2005). The strength of receptor signaling is centrally controlled through a cooperative loop between Ca2+ and an oxidant signal. *Cell*, **121**, 281–293.
34. Kim, J. R., Kwon, K. S., Yoon, H. W., Lee, S. R. & Rhee, S. G. (2002). Oxidation of proteinaceous cysteine residues by dopamine-derived H2O2 in PC12 cells. *Arch. Biochem. Biophys.* **397**, 414–423.
35. O'Donoghue, S. I., Miki, M. & dos Remedios, C. G. (1992). Removing the two C-terminal residues of actin affects the filament structure. *Arch. Biochem. Biophys.* **293**, 110–116.
36. Holmes, K. C., Popp, D., Gebhard, W. & Kabsch, W. (1990). Atomic model of the actin filament. *Nature*, **347**, 44–49.
37. Weik, M., Ravelli, R. B., Kryger, G., McSweeney, S., Raves, M. L., Harel, M. *et al.* (2000). Specific chemical and structural damage to proteins produced by synchrotron radiation. *Proc. Natl Acad. Sci. USA*, **97**, 623–628.
38. Bagley, S. C. & Altman, R. B. (1995). Characterizing the microenvironment surrounding protein sites. *Protein Sci.* **4**, 622–635.
39. Tirion, M. M., ben-Avraham, D., Lorenz, M. & Holmes, K. C. (1995). Normal modes as refinement parameters for the F-actin model. *Biophys. J.* **68**, 5–12.
40. Rould, M. A., Wan, Q., Joel, P. B., Lowey, S. & Trybus, K. M. (2006). Crystal structures of expressed non-polymerizable monomeric actin in the ADP and ATP states. *J. Biol. Chem.* **281**, 31909–31919.
41. Vorobiev, S., Strokopytov, B., Drubin, D. G., Frieden, C., Ono, S., Condeelis, J. *et al.* (2003). The structure of nonvertebrate actin: implications for the ATP hydrolytic mechanism. *Proc. Natl Acad. Sci. USA*, **100**, 5760–5765.
42. Klenchin, V. A., Khaitlina, S. Y. & Rayment, I. (2006). Crystal structure of polymerization-competent actin. *J. Mol. Biol.* **362**, 140–150.
43. Bhattacharyya, R., Pal, D. & Chakrabarti, P. (2004). Disulfide bonds, their stereospecific environment and conservation in protein structures. *Protein Eng. Des. Sel.* **17**, 795–808.
44. Hesterkamp, T., Weeds, A. G. & Mannherz, H. G. (1993). The actin monomers in the ternary gelsolin: 2 actin complex are in an antiparallel orientation. *Eur. J. Biochem.* **218**, 507–513.
45. Millonig, R., Salvo, H. & Aebi, U. (1988). Probing actin polymerization by intermolecular cross-linking. *J. Cell Biol.* **106**, 785–796.
46. Mockrin, S. C. & Korn, E. D. (1981). Isolation and characterization of covalently cross-linked actin dimer. *J. Biol. Chem.* **256**, 8228–8233.
47. Schoenenberger, C. A., Bischler, N., Fahrenkrog, B. & Aebi, U. (2002). Actins propensity for dynamic filament patterning. *FEBS Letters*, **529**, 27–33.
48. Tang, J. X., Janmey, P. A., Stossel, T. P. & Ito, T. (1999). Thiol oxidation of actin produces dimers that enhance the elasticity of the F-actin network. *Biophys. J.* **76**, 2208–2215.
49. Bubb, M. R., Govindasamy, L., Yarmola, E. G., Vorobiev, S. M., Almo, S. C., Somasundaram, T. *et al.* (2002). Polylysine induces an antiparallel actin dimer that nucleates filament assembly: crystal structure at 3.5-Å resolution. *J. Biol. Chem.* **277**, 20999–21006.
50. Margarit, S. M., Davidson, W., Frego, L. & Stebbins, C. (2006). A steric antagonism of actin polymerization by a Salmonella virulence protein. *Structure*, **14**, 1219–1229.
51. Reutzel, R., Yoshioka, C., Govindasamy, L., Yarmola, E. G., Agbandje-McKenna, M., Bubb, M. R. & McKenna, R. (2004). Actin crystal dynamics: structural implications for F-actin nucleation, polymerization, and branching mediated by the anti-parallel dimer. *J. Struct. Biol.* **146**, 291–301.
52. Blundell, T. L. & Fernandez-Recio, J. (2006). Cell biology: brief encounters bolster contacts. *Nature*, **444**, 279–280.
53. Goley, E. D. & Welch, M. D. (2006). The ARP2/3 complex: an actin nucleator comes of age. *Nature Rev. Mol. Cell Biol.* **7**, 713–726.
54. Steinmetz, M. O., Goldie, K. N. & Aebi, U. (1997). A correlative analysis of actin filament assembly, structure, and dynamics. *J. Cell Biol.* **138**, 559–574.
55. Le Clainche, C., Pantaloni, D. & Carlier, M. F. (2003). ATP hydrolysis on actin-related protein 2/3 complex causes debranching of dendritic actin arrays. *Proc. Natl Acad. Sci. USA*, **100**, 6337–6342.
56. Choi, M. H., Lee, I. K., Kim, G. W., Kim, B. U., Han, Y. H., Yu, D. Y. *et al.* (2005). Regulation of PDGF signalling and vascular remodelling by peroxiredoxin II. *Nature*, **435**, 347–353.
57. Rhee, S. G., Bae, Y. S., Lee, S. R. & Kwon, J. (2000). Hydrogen peroxide: a key messenger that modulates protein phosphorylation through cysteine oxidation. *Sci. STKE*, **2000**, PE1.
58. Hu, T., Ramachandrarao, S. P., Siva, S., Valancius, C., Zhu, Y., Mahadev, K. *et al.* (2005). Reactive oxygen species production via NADPH oxidase mediates TGF-beta-induced cytoskeletal alterations in endothelial cells. *Am. J. Physiol. Renal Physiol.* **289**, F816–F825.
59. Radmark, O. & Samuelsson, B. (2005). Regulation of

5-lipoxygenase enzyme activity. *Biochem. Biophys. Res. Commun.* **338**, 102–110.
60. Li, J. M. & Shah, A. M. (2002). Intracellular localization and preassembly of the NADPH oxidase complex in cultured endothelial cells. *J. Biol. Chem.* **277**, 19952–19960.
61. Provost, P., Doucet, J., Hammarberg, T., Gerisch, G., Samuelsson, B. & Radmark, O. (2001). 5-Lipoxygenase interacts with coactosin-like protein. *J. Biol. Chem.* **276**, 16520–16527.
62. Abo, A., Pick, E., Hall, A., Totty, N., Teahan, C. G. & Segal, A. W. (1991). Activation of the NADPH oxidase involves the small GTP-binding protein p21rac1. *Nature*, **353**, 668–670.
63. Moldovan, L., Irani, K., Moldovan, N. I., Finkel, T. & Goldschmidt-Clermont, P. J. (1999). The actin cytoskeleton reorganization induced by Rac1 requires the production of superoxide. *Antioxid Redox Signal*, **1**, 29–43.
64. Irani, K., Xia, Y., Zweier, J. L., Sollott, S. J., Der, C. J., Fearon, E. R. *et al.* (1997). Mitogenic signaling mediated by oxidants in Ras-transformed fibroblasts. *Science*, **275**, 1649–1652.
65. Meili, R. & Firtel, R. A. (2003). Two poles and a compass. *Cell*, **114**, 153–156.
66. Kraynov, V. S., Chamberlain, C., Bokoch, G. M., Schwartz, M. A., Slabaugh, S. & Hahn, K. M. (2000). Localized Rac activation dynamics visualized in living cells. *Science*, **290**, 333–337.
67. Rhee, S. G., Kang, S. W., Jeong, W., Chang, T. S., Yang, K. S. & Woo, H. A. (2005). Intracellular messenger function of hydrogen peroxide and its regulation by peroxiredoxins. *Curr. Opin. Cell Biol.* **17**, 183–189.
68. Bae, Y. S., Sung, J. Y., Kim, O. S., Kim, Y. J., Hur, K. C., Kazlauskas, A. & Rhee, S. G. (2000). Platelet-derived growth factor-induced H(2)O(2) production requires the activation of phosphatidylinositol 3-kinase. *J. Biol. Chem.* **275**, 10527–10531.
69. Hall, A. (1998). Rho GTPases and the actin cytoskeleton. *Science*, **279**, 509–514.
70. Lassing, I. & Lindberg, U. (1990). Polyphosphoinositide synthesis in platelets stimulated with low concentrations of thrombin is enhanced before the activation of phospholipase C. *FEBS Letters*, **262**, 231–233.
71. Chong, L. D., Traynor-Kaplan, A., Bokoch, G. M. & Schwartz, M. A. (1994). The small GTP-binding protein Rho regulates a phosphatidylinositol 4-phosphate 5-kinase in mammalian cells. *Cell*, **79**, 507–513.
72. Karlsson, R., Lassing, I., Hoglund, A. S. & Lindberg, U. (1984). The organization of microfilaments in spreading platelets: a comparison with fibroblasts and glial cells. *J. Cell Physiol.* **121**, 96–113.
73. Mellstroom, K., Hoglund, A. S., Nister, M., Heldin, C. H., Westermark, B. & Lindberg, U. (1983). The effect of platelet-derived growth factor on morphology and motility of human glial cells. *J. Muscle Res. Cell Motil.* **4**, 589–609.
74. Rozelle, A. L., Machesky, L. M., Yamamoto, M., Driessens, M. H., Insall, R. H., Roth, M. G. *et al.* (2000). Phosphatidylinositol 4,5-bisphosphate induces actin-based movement of raft-enriched vesicles through WASP-Arp2/3. *Curr. Biol.* **10**, 311–320.
75. Ackermann, M. & Matus, A. (2003). Activity-induced targeting of profilin and stabilization of dendritic spine morphology. *Nature Neurosci.* **6**, 1194–2100.
76. Chiarugi, P., Pani, G., Giannoni, E., Taddei, L., Colavitti, R., Raugei, G. *et al.* (2003). Reactive oxygen species as essential mediators of cell adhesion: the oxidative inhibition of a FAK tyrosine phosphatase is required for cell adhesion. *J. Cell Biol.* **161**, 933–944.
77. Finkel, T. & Holbrook, N. J. (2000). Oxidants, oxidative stress and the biology of ageing. *Nature*, **408**, 239–247.
78. Schulz, J. B., Lindenau, J., Seyfried, J. & Dichgans, J. (2000). Glutathione, oxidative stress and neurodegeneration. *Eur. J. Biochem.* **267**, 4904–4911.
79. Finkel, T. (2005). Opinion: Radical medicine: treating ageing to cure disease. *Nature Rev. Mol. Cell Biol.* **6**, 971–976.
80. Aksenov, M. Y., Aksenova, M. V., Butterfield, D. A., Geddes, J. W. & Markesbery, W. R. (2001). Protein oxidation in the brain in Alzheimer's disease. *Neuroscience*, **103**, 373–383.
81. Kwon, C. H., Luikart, B. W., Powell, C. M., Zhou, J., Matheny, S. A., Zhang, W. *et al.* (2006). Pten regulates neuronal arborization and social interaction in mice. *Neuron*, **50**, 377–388.
82. Holmgren, A. & Bjornstedt, M. (1995). Thioredoxin and thioredoxin reductase. *Methods Enzymol.* **252**, 199–208.
83. Schüler, H., Karlsson, R. & Lindberg, U. (2006). Purification of nonmuscle actin. In *Cell Biology: A Laboratory Handbook* (Celis, J., ed.) vol 2, pp. 165–171. Elsevier Science, New York.
84. Pardee, J. D. & Spudich, J. A. (1982). Purification of muscle actin. *Methods Enzymol.* **85**, 164–181.
85. Houk, T. W., Jr & Ue, K. (1974). The measurement of actin concentration in solution: a comparison of methods. *Anal. Biochem.* **62**, 66–74.
86. Laemmli, U. K. (1970). Cleavage of structural proteins during the assembly of the head of bacteriophage T4. *Nature*, **227**, 680–685.
87. Ellman, G. L. (1959). Tissue sulfhydryl groups. *Arch. Biochem. Biophys.* **82**, 70–77.
88. Kouyama, T. & Mihashi, K. (1981). Fluorimetry study of N-(1-pyrenyl)iodoacetamide-labelled F-actin. Local structural change of actin protomer both on polymerization and on binding of heavy meromyosin. *Eur. J. Biochem.* **114**, 33–38.
89. Kabsch, W. (1993). Automatic processing of rotation diffraction data from crystals and initially unknown symmetry and cell constants. *J. Appl. Crystallog.* **26**, 795–800.
90. Collaborative Computational Project, Number 4. (1994). The CCP4 suite: programs for protein crystallography. *Acta Crystallog. sect. D*, **50**, 760–763.
91. McCoy, A. J., Grosse-Kunstleve, R. W., Storoni, L. C. & Read, R. J. (2005). Likelihood-enhanced fast translation functions. *Acta Crystallog. sect. D*, **61**, 458–464.
92. Otterbein, L. R., Graceffa, P. & Dominguez, R. (2001). The crystal structure of uncomplexed actin in the ADP state. *Science*, **293**, 708–711.
93. Brunger, A. T., Adams, P. D., Clore, G. M., DeLano, W. L., Gros, P., Grosse-Kunstleve, R. W. *et al.* (1998). Crystallography & NMR system: a new software suite for macromolecular structure determination. *Acta Crystallog. sect. D*, **54**, 905–921.
94. Murshudov, G. N., Vagin, A. A. & Dodson, E. J. (1997). Refinement of macromolecular structures by the maximum-likelihood method. *Acta Crystallog. sect. D*, **53**, 240–255.
95. Brunger, A. T. (1992). Free R value: a novel statistical quantity for assessing the accuracy of crystal structures. *Nature*, **355**, 472–475.
96. Emsley, P. & Cowtan, K. (2004). Coot: model-building tools for molecular graphics. *Acta Crystallog. sect. D*, **60**, 2126–2132.

97. Winn, M. D., Isupov, M. N. & Murshudov, G. N. (2001). Use of TLS parameters to model anisotropic displacements in macromolecular refinement. *Acta Crystallog. sect. D*, **57**, 122–133.
98. Schuttelkopf, A. W. & van Aalten, D. M. (2004). PRODRG: a tool for high-throughput crystallography of protein-ligand complexes. *Acta Crystallog. sect. D*, **60**, 1355–1363.
99. Lovell, S. C., Davis, I. W., Arendall, W. B., 3rd, de Bakker, P. I., Word, J. M., Prisant, M. G. *et al.* (2003). Structure validation by Calpha geometry: phi,psi and Cbeta deviation. *Proteins: Struct. Funct. Genet.* **50**, 437–450.
100. Vagin, A. A., Richelle, J. & Wodak, S. J. (1999). SFCHECK: a unified set of procedures for evaluating the quality of macromolecular structure-factor data and their agreement with the atomic model. *Acta Crystallog. sect. D*, **55**, 191–205.
101. Hooft, R. W., Vriend, G., Sander, C. & Abola, E. E. (1996). Errors in protein structures. *Nature*, **381**, 272.
102. Jones, S. & Thornton, J. M. (1996). Principles of protein-protein interactions. *Proc. Natl Acad. Sci. USA*, **93**, 13–20.
103. Krissinel, E. & Henrick, K. (2005). Detection of Protein Assemblies in Crystals. *In Protein Interfaces, Surfaces and Assemblies Service PISA at European Bioinformatics Institute. CompLife 2005.* Springer, Berlin-Heidelberg.
104. Kabsch, W., Mannherz, H. G., Suck, D., Pai, E. F. & Holmes, K. C. (1990). Atomic structure of the actin: DNase I complex. *Nature*, **347**, 37–44.

Edited by I. Wilson

(Received 8 February 2007; received in revised form 18 April 2007; accepted 18 April 2007)
Available online 4 May 2007